

Kinetic study on photocatalytic hydrogenation of acetophenone derivatives on titanium dioxide†

Cite this: *Catal. Sci. Technol.*, 2014, 4, 1084

Shigeru Kohtani,* Yuna Kamoi, Eito Yoshioka and Hideto Miyabe*

Acetophenone (AP) derivatives were photocatalytically hydrogenated to afford the corresponding secondary alcohols with excellent chemical efficiencies on titanium dioxide (Degussa P25, TiO₂) under UV light irradiation. Maximum reaction rates (k_{\max}) and apparent adsorption constants (K_{LH}) under irradiation were obtained from the Langmuir–Hinshelwood kinetic analysis. The k_{\max} values showed a tendency to decrease with the decreasing reduction potentials (E_{red}) of the AP derivatives, while the K_{LH} values were distributed in the range of 280–780 L mol⁻¹. Among these, simple AP exhibited the greatest adsorptivity upon the UV irradiated TiO₂ surface. Additionally, it was demonstrated that the electrons trapped at surface defect Ti (Ti_{st}) sites on the TiO₂ actually hydrogenated the AP derivatives. The amount of reacted electrons also showed a tendency to decrease with decreasing E_{red} values, in accord with the dependence on k_{\max} . These results indicate that the electrons accumulated at shallow Ti_{st} states easily participate in the hydrogenation of AP derivatives, whereas those trapped at deeper states hardly react with the substrates. The results strongly support the electron transfer reaction model *via* the Ti_{st} sites in the photocatalytic hydrogenation on TiO₂.

Received 3rd November 2013,
Accepted 7th January 2014

DOI: 10.1039/c3cy00879g

www.rsc.org/catalysis

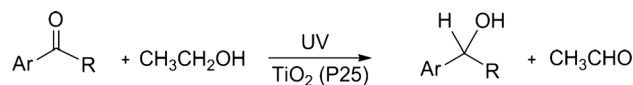
Introduction

Some metal oxides (*e.g.* titanium dioxide (TiO₂)) are regarded as semiconductors, in which electrons (e⁻) photogenerated in the conduction band (CB) and holes (h⁺) simultaneously generated in the valence band (VB) play important roles in chemical transformations as e⁻ and h⁺ can induce redox reactions on the surface. Photocatalytic hydrogenation on such semiconductor particles proceeds *via* electron transfer into a substrate followed by protonation. In general, photo-hydrogenation can take place in the presence of a large excess amount of electron donors, such as water, alcohols or amines, and in the absence of molecular oxygen (O₂). The aim of using an electron donor is to scavenge h⁺ generated in the VB, thereby diminishing the degree of recombination between e⁻ and h⁺ within the particles.

Photocatalytic hydrogenation has received increasing attention as a new method for the synthetically useful reduction of organic compounds having various double or triple bonds.^{1–6} This methodology has some advantages compared to conventional reduction methods: (1) the most important merit is that particular reducing agents (*e.g.* H₂ gas, NaBH₄, LiAlH₄ *etc.*) are not necessary. In most cases, the reductants

are conventional solvents, such as water or alcohols, which concurrently act as h⁺ scavengers, as mentioned above. Therefore, this method allows us to avoid both the use of harmful and dangerous chemical reagents and the emission of harmful waste. (2) The reactions mostly proceed under mild conditions, *e.g.* under ordinary temperature and pressure, and therefore are safe. (3) In the case of TiO₂ or other stable metal oxide photocatalysts, the materials are chemically stable, easily removable, and reusable. These significant advantages imply that this methodology holds great promise to become an alternative “green” synthetic method for reductive chemical transformations.

We have recently reported that acetophenone (AP) derivatives can be photocatalytically hydrogenated to afford the corresponding secondary alcohols on Degussa P25 TiO₂ powders under UV light irradiation (Scheme 1).² The desired secondary alcohols were obtained with excellent chemical efficiency, almost 100% yields, by choosing ethanol as a sacrificial h⁺ scavenger, which was oxidized to acetaldehyde. More recently, we have demonstrated that some AP derivatives can be hydrogenated on P25 TiO₂ powder modified with organic dyes under visible light irradiation.³ In the study,



Scheme 1 Photocatalytic hydrogenation of AP derivatives: Ar = aromatic ring, R = H, Me, Et, *i*-Pr, or CF₃.

Department of Pharmacy, School of Pharmacy, Hyogo University of Health Sciences, 1-3-6, Minatojima, Chuo-ku, Kobe, 650-8530, Japan. E-mail: kohtani@huhs.ac.jp, miyabe@huhs.ac.jp; Fax: +81 78 304 2858; Tel: +81 78 304 3158

† Electronic supplementary information (ESI) available. See DOI: 10.1039/c3cy00879g

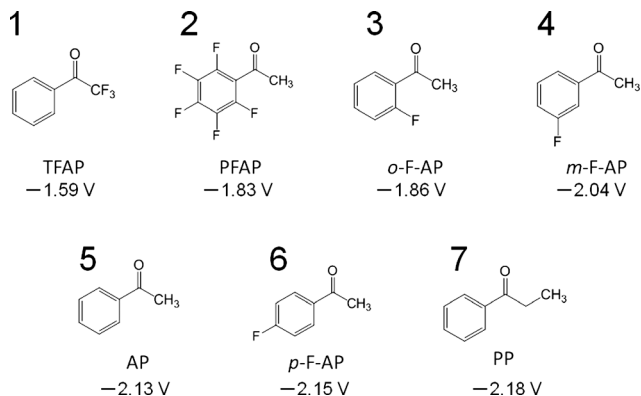


Fig. 1 Reduction potential of AP derivatives vs. SHE in acetonitrile.²

we found that a suitable combination of dye-TiO₂ and triethylamine as a sacrificial electron donor successfully extended the UV response of TiO₂ towards the visible light region. We have further examined the adsorptive and kinetic behavior in the photocatalytic hydrogenation of AP 5 and 2,2,2-trifluoroacetophenone (TFAP) 1 upon the UV irradiated TiO₂ surface.⁴ The study showed that the trapped electrons at surface defect (Ti_{st}) sites^{7–9} actually take part in the hydrogenation of AP 5 and TFAP 1. Therefore, it is important for us to prove the generality of the electron transfer reaction *via* the Ti_{st} sites for other AP derivatives in photocatalytic hydrogenation.

For this purpose, we selected seven AP derivatives, 1–7, with different reduction potentials (E_{red} vs. Standard Hydrogen Electrode, SHE), depicted in Fig. 1, and investigated the dependence of E_{red} on the hydrogenation efficiency. Here, maximum reaction rates (k_{max}) and apparent adsorption constants (K_{LH}) under UV irradiation were determined by the Langmuir–Hinshelwood (LH) kinetic analysis. Furthermore, the molar amount of reacted electrons trapped at Ti_{st} with the AP derivatives was also estimated using a pre-irradiated TiO₂ system. On the basis of these data, a reasonable electron transfer model *via* the Ti_{st} sites will be proposed in the TiO₂-catalyzed photo-hydrogenation of AP derivatives.

Materials and methods

2.1 Materials

The TiO₂ powder (Degussa P25, specific surface area: 35–65 m² g⁻¹) was used as received. HPLC grade ethanol was purchased from Nacalai Tesque and used without further purification. The following reagents were used as substrates and their quantification on gas chromatography (GC) as received: 2,2,2-trifluoroacetophenone (1, TFAP, Aldrich, 99%), 2',3',4',5',6'-pentafluoroacetophenone (2, PFAP, Aldrich, 97%), 2'-fluoroacetophenone (3, *o*-F-AP, Aldrich, 97%), 3'-fluoroacetophenone (4, *m*-F-AP, Aldrich, 97%), acetophenone (5, AP, Nacalai Tesque, 98.5%), 4'-fluoroacetophenone (6, *p*-F-AP, Aldrich, 99%), propiophenone (7, PP, Aldrich, 99%). The following reagents were used for the identification and quantification of the desired products

without further purification: 1-phenyl-2,2,2-trifluoroethanol (Aldrich, 98%), 1-(2',3',4',5',6'-pentafluorophenyl)ethanol (Aldrich, 97%), 1-(2'-fluorophenyl)ethanol (Aldrich, 97%), 1-(3'-fluorophenyl)ethanol (Avocado, 97%), 1-phenylethanol (TCI, >98.0%), 1-(4'-fluorophenyl)ethanol (Avocado, 99%), and 1-phenyl-1-propanol (TCI, >97.0%).

2.2 Prolonged UV irradiation experiment

Irradiation experiments were carried out for a mixture of the AP derivatives (initial concentration range: 1–20 mmol L⁻¹) and TiO₂ (0.10 g) in a deaerated ethanol solution (30 mL) under irradiation with UV light (>350 nm, light intensity: 790 mW cm⁻²) at 305 K. The details of the irradiation experiment and GC analysis have been described in our previous reports.^{2,4}

2.3 Pre-UV irradiation experiment

The TiO₂ powder (0.10 g) was dispersed in ethanol (30 mL) and this suspension was degassed with argon bubbling for at least 30 min. After the degassed solution was irradiated with UV light (>350 nm, light intensity: 1280 mW cm⁻²) for 2 h, the white color of the TiO₂ powder changed into blue–gray. After confirming the color change, 300 μmol of the AP derivatives was injected into this TiO₂ suspension in the dark. Then, electron transfer from the Ti_{st} sites to the adsorbed AP derivatives took place and afforded the corresponding secondary alcohols. The amounts of the products were quantitatively analyzed by GC-MS.⁴

2.4 Quantum chemical calculations

Density functional theory (DFT) calculations were performed with Spartan'10 at the B3LYP/6-31+G* level of theory. Electrostatic potential energy maps of the AP derivatives were obtained when the geometry optimizations were achieved, which were evaluated by the heat of formation.

Results and discussion

3.1 Photocatalytic hydrogenation during the prolonged UV irradiation

Fig. 2 shows the time profiles of the photocatalytic hydrogenation at several initial concentrations of *o*-F-AP 3 as a representative AP derivative. The time dependence on the decays of 3 (Fig. 2(a)) and the formation of the corresponding secondary alcohol (Fig. 2(b)) indicate very similar features to those reported for AP:⁴ (1) the hydrogenation reaction proceeds almost quantitatively, (2) the time dependence shows a linear relationship between the concentration and irradiation time in the high concentration region, suggesting zero-order rate dependence at high concentration, and (3) the slopes of the time profiles become smaller with a decreasing concentration of 3, implying that the kinetic behavior varies from zero- to first-order depending on the concentration of 3. Other substrates 2, 4, 6, and 7 also exhibited similar time dependence except for 1 (see: Fig. S1–S4 in the ESI†).

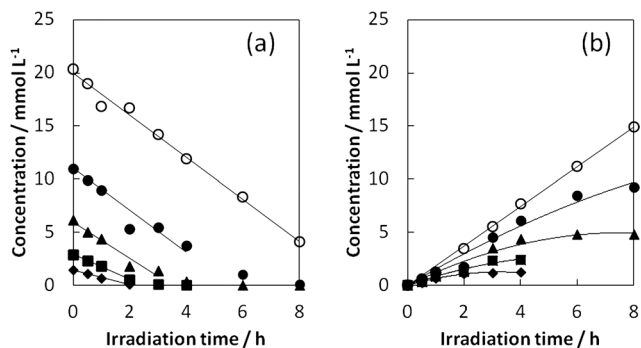


Fig. 2 Time profiles of (a) the decay of *o*-F-AP 3 and (b) the formation of the corresponding secondary alcohol in ethanol under the irradiation conditions (>350 nm, 790 mW cm⁻²) at 305 K.

Fig. 3 depicts the initial reaction rates, v_0 , (the slopes in Fig. 2(a)) vs. the initial concentration of the substrates in ethanol at 305 K. The rates, v_0 , increase to attain maximum values asymptotically with increasing concentration in solution. These data are well analyzed by the LH kinetic expression (1):

$$v_0 = \frac{k_{\max} K_{\text{LH}} C_0}{1 + K_{\text{LH}} C_0} \quad (1)$$

where v_0 is the initial reaction rate, k_{\max} is the maximum value of the reaction rate, K_{LH} is the apparent adsorption constant under irradiation, and C_0 is the initial concentration of the AP derivatives in equilibrium. The best fitting parameters are listed in Table 1. The k_{\max} values for 2–7 obtained from the LH kinetic analysis show a tendency to decrease with decreasing E_{red} of the AP derivatives. On the other hand, the photo-hydrogenation of 1 followed the first-order rate law because of the predominant formation of ketal or hemiketal species in ethanol, *i.e.*, only a few percent of 1 remained in the original keto form.⁴ Thus, the k_{\max} value for 1 is not evaluated in this study. On the contrary, neither the formation of

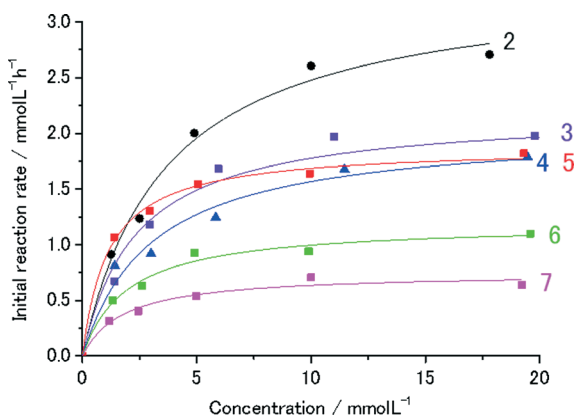


Fig. 3 Dependencies of the initial rates (v_0) of hydrogenation at the initial concentration of the six AP derivatives (2–7) under UV irradiation (>350 nm, light intensity: 790 mW cm⁻²) at 305 K. These data were fitted by eqn (1): $v_0 = k_{\max} K_{\text{LH}} C_0 / (1 + K_{\text{LH}} C_0)$. The best fitting parameters are listed in Table 1.

ketal nor hemiketal species was observed for substrates 2–7. Accordingly, common kinetic behavior was confirmed for the AP derivatives 2–7.

The results listed in Table 1 indicate that E_{red} seems to correlate with k_{\max} but not with K_{LH} . The K_{LH} values are distributed in the range of 280–780 L mol⁻¹, which are associated with adsorptivity onto the TiO₂ surface under UV irradiation. Henderson proposed the major adsorption state of acetone on a rutile TiO₂ (110) single crystal on the basis of high-resolution electron energy-loss spectroscopy, in which acetone presumably binds at Ti⁴⁺ sites *via* the lone pair on the oxygen atom of acetone (η_1 geometry).^{9,10} Later, he and his co-workers calculated the adsorption energy for various carbonyl compounds, including AP, using the DFT method and obtained a sufficient negative adsorption energy for AP (-77 kJ mol⁻¹),¹¹ suggesting the presence of η_1 species on the rutile TiO₂ (110) surface. A similar adsorption model can also be adapted to our system. We calculated the electrostatic potential energy map of the AP derivatives 2–7 using the DFT method (see Fig. S5 in the ESI†). The calculated electrostatic potential energy on the oxygen atom seems to be well correlated with the K_{LH} values (Table 1), meaning that the AP derivatives would most likely adsorb onto the surface Ti⁴⁺ sites with similar η_1 geometry. The K_{LH} value for AP 5 is larger than that for PP 7, while the electrostatic potential energy for AP 5 and PP 7 shows almost the same value (*ca.* -180 kJ mol⁻¹). This discrepancy may be explained in terms of the UV-induced super-hydrophilic TiO₂ surface.^{8,9,12} The hydrophobicity of organic compounds can be evaluated by the octanol–water partition coefficient (P). The found values of $\log P$ for AP 5 and PP 7 are reported to be 1.58 and 2.19, respectively.¹³ This inversely implies that the hydrophilicity of AP 5 is greater than that of PP 7, which therefore should become a great advantage for the adsorption of AP 5 onto the super-hydrophilic TiO₂ surface.

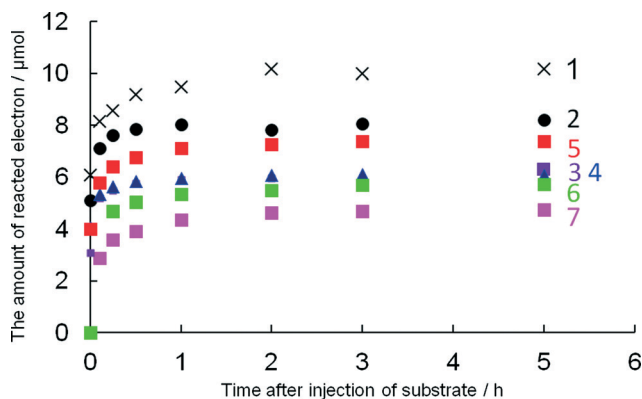
3.2 Electron transfer efficiency on the pre-irradiated TiO₂ surface

The electron transfer efficiency from the surface defect Ti_{st} to the adsorbed AP derivatives on TiO₂ was evaluated by the injection experiment for a pre-irradiated TiO₂ suspension.⁴ It is well known that there are various Ti_{st} sites, for example, the five coordinate Ti and the O vacancies on the TiO₂ surface and so on.^{7–9} The electronic energy of the Ti_{st} states is almost located just below the CB edge of TiO₂ in the range of *ca.* 1 eV.⁹ Therefore, electrons excited in the CB band should relax to the Ti_{st}⁴⁺ sites to yield the accumulated electrons (Ti_{st}³⁺), which are indicated by the blue–gray color with an absorption band from the visible to the IR region.^{14–19} After being confirmed by the color change from white to blue–gray in the 2 h pre-irradiation of the TiO₂ suspension, a sufficient amount of each AP derivative was injected into this suspension in the dark so that the surface electron transfer from Ti_{st}³⁺ to the adsorbed AP derivatives took place to afford the corresponding secondary alcohols.⁴ Fig. 4 shows plots of the

Table 1 Reduction potentials, best fitting parameters for the LH kinetic expression (1), and the electrostatic potential energy on the oxygen atom of the AP derivatives

Substrate	$E_{\text{red}}^a/\text{V}$	$k_{\text{max}}/10^{-3} \text{ mol L}^{-1} \text{ h}^{-1}$	$K_{\text{LH}}/\text{L mol}^{-1}$	Potential energy ^b /kJ mol ⁻¹
2	-1.59	3.4 ± 0.2	280 ± 50	-147.4
3	-1.62	2.2 ± 0.2	420 ± 100	-173.2
4	-1.80	2.0 ± 0.1	330 ± 90	-168.4
5	-1.89	1.9 ± 0.1	780 ± 90	-180.5
6	-1.92	1.2 ± 0.1	510 ± 90	-172.4
7	-1.94	0.75 ± 0.05	560 ± 110	-178.4

^a Reduction potential vs. SHE determined by cyclic voltammetry in CH₃CN containing a Bu₄NClO₄ supporting electrolyte, in which the standard potential of the Ag wire reference electrode used was compensated by the potential of the Fc⁺/Fc couple vs. SHE.² ^b Calculated using the DFT method (B3LYP/6-31+G*).

**Fig. 4** Time evolutions of the molar amount of reacted electrons after the injection of substrate 1-7 (300 μmol) into the 2 h pre-irradiated TiO₂ suspension at 305 K.

molar amount of reacted electrons after the injection of each of the seven substrates. The amount of reacted electrons first grew up and almost reached a constant value after 3 h. Just for information, the amount of reacted electrons is two times larger than that of the secondary alcohols, because the single electron transfer takes place twice in the hydrogenation.

Although TFAP **1** gives the ketal or hemiketal form in ethanol in equilibrium, a sufficient concentration of the keto form of **1** (*ca.* 10 mmol L⁻¹) near the TiO₂ surface can be attained immediately after the injection of **1**, because it survives as the keto form for about ten minutes at 305 K.⁴ In addition, we found that all of the accumulated electrons at

Ti_{st}³⁺ were consumed for the reductive hydrogenation of **1** because the color change of TiO₂ from blue-gray to white completed within 3 h after the injection of **1**.⁴ Therefore, the total amount of Ti_{st}³⁺ generated on the TiO₂ powder was estimated to be *ca.* 100 μmol g⁻¹ after 5 h (the plots for **1** in Fig. 4). This value is roughly consistent with the reported one (50 μmol g⁻¹), determined using the surface reaction of Ti³⁺ with methylviologen to afford its cation radical on the P25 TiO₂ powder in a deaerated aqueous solution containing methanol as a sacrificial reagent.²⁰ On the other hand, in the case of the other AP derivatives 2-7, part of the blue-gray species on TiO₂ remained even 5 h after the AP derivatives were injected, which must be due to the deeply trapped electrons at Ti_{st}³⁺ remaining on the P25 TiO₂ powder. This means that the electrons accumulated at the shallow defect states easily participate in the reduction of the AP derivatives 2-7, whereas those trapped at deeper states hardly transfer on the TiO₂ surface. Assuming that all of the accumulated electrons react with **1** on the TiO₂ surface, the percentages of reacted electrons were estimated for the other AP derivatives, as summarized in Table 2. The values roughly depend on E_{red} except for AP **5**. The upward deviation for AP **5** may be due to the greater adsorptivity, as mentioned in the previous section.

3.3 Reaction model on the TiO₂ surface

Fig. 5 indicates the dependencies of the amount of reacted electrons (several μmol) and the maximum reaction rates (k_{max}) on E_{red} for the seven AP derivatives 1-7. The amount of

Table 2 Reduction potentials, the amount of reacted electrons at 5 h, and percentages of reacted electrons^a

Substrate	$E_{\text{red}}/\text{V}^b$	The amount of reacted electrons/μmol	Percentage ^c /%
1	-1.35	10.2	100
2	-1.59	8.22	81
3	-1.62	6.32	62
4	-1.80	6.09	60
5	-1.89	7.38	72
6	-1.92	5.70	56
7	-1.94	4.76	47

^a The molar amount of reacted electrons was estimated at 5 h after the injection of substrate 1-7 (300 μmol) into the 2 h pre-irradiated TiO₂ suspension at 305 K. ^b Reduction potential vs. SHE (see the footnote in Table 1). ^c Percentage of the reacted electrons per the total amount of Ti_{st}³⁺ (10.2 μmol) generated on 0.10 g of the TiO₂.

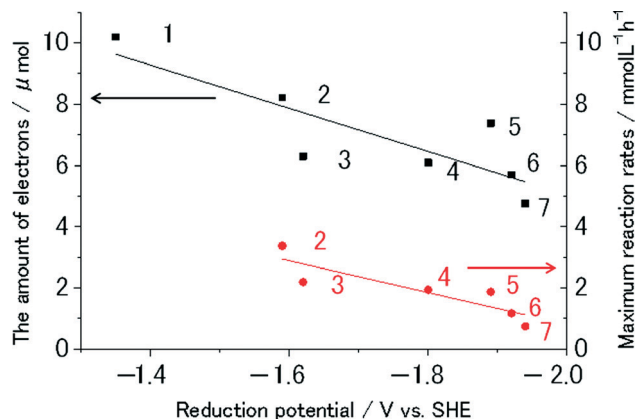


Fig. 5 The dependencies of the amount of reacted electrons (■) and k_{\max} (●) on E_{red} for the seven AP derivatives 1–7.

reacted electrons showed a tendency in decrease on decreasing the E_{red} values, in accord with the dependence on k_{\max} . Thus, the k_{\max} values of the AP derivatives show a strong correlation with the amount of reacted electrons on the pre-irradiated TiO_2 surface. This implies that the rates of photocatalytic hydrogenation of the AP derivatives are governed by the electron transfer efficiency from the Ti_{st} sites to the adsorbed AP ones.

Let us consider the dependence of k_{\max} on E_{red} and the relationship between k_{\max} and the amount of reacted electrons on the basis of the Marcus theory at the semiconductor/liquid interface.^{21–24} From the result of the good correlation between k_{\max} and the amount of reacted electrons (Fig. 5), the reaction rate for AP derivatives possessing different E_{red} is supposed to be closely associated with the electronic energy of Ti_{st} states and their distribution within the band gap. However, it is difficult to obtain information about the energy distribution of Ti_{st} states on the actual TiO_2 surface. Ondersma and Hamann have recently applied this theory to the model of electron transfer recombination between a nanoparticle TiO_2 electrode and redox shuttle.²⁴ A similar model can be illustrated for our electron transfer reaction, as shown in Fig. 6, where the fluctuating energy levels for the adsorbed acceptor (solid line: neutral AP derivatives) and donor (broken line: their anionic species) are indicated in accordance with the Marcus theory. In this model, when the AP derivatives fully adsorb onto the Ti_{st} sites and show the maximum coverage, the contributions to the reaction rate from all the occupied Ti_{st} states must be included in the net electron transfer rate, k_{\max} , which is therefore integrated from the bottom energy of the Ti_{st} states (E_{b}) to the band edge of the CB (E_{cb}) as follows:

$$k_{\max} \propto \int_{E_{\text{b}}}^{E_{\text{cb}}} g(E) f(E - E_{\text{F}}) k_{\text{et}}(E) dE \quad (2)$$

where $g(E)$ is the density of surface trap states, $f(E - E_{\text{F}})$ is the Fermi–Dirac function indicating the trap state occupancy at a given Fermi level E_{F} , and $k_{\text{et}}(E)$ is the electron transfer rate constant from a surface Ti_{st} state at energy E given by

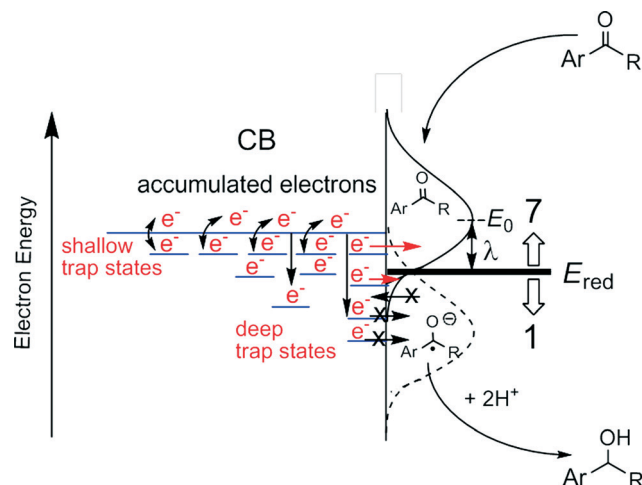


Fig. 6 Schematic illustration of the electron transfer reaction from the Ti_{st} sites to the adsorbed AP derivatives, where E_{red} is the reduction potential of the AP derivative, λ is the reorganization energy (ca. 0.7 eV),²⁵ and $E_0 (= qE_{\text{red}} - \lambda)$ is the energy at the top of the curve for the acceptor level (solid line). The dotted line indicates the donor energy level for the anionic species of the AP derivatives.

$$k_{\text{et}}(E) = k_{\text{et}}(E_0) \exp \left[\frac{-(E - qE_{\text{red}} + \lambda)^2}{4\lambda k_{\text{B}} T} \right] \quad (3)$$

where λ is the reorganization energy of the acceptor species near the TiO_2 surface, which is the sum of the inner-sphere and outer-sphere components,^{21–24} q is the charge of an electron, k_{B} is the Boltzmann's constant, and T is the temperature. $k_{\text{et}}(E)$ also contains the electronic coupling term, which may inherently differ between types of Ti_{st} states and the adsorbed AP derivatives but is assumed here to be independent of the energy over the range of interest, as previously reported.^{22–24} When E is $E_0 (= qE_{\text{red}} - \lambda)$ at the top of the curve of the acceptor level (solid line), $k_{\text{et}}(E_0)$ exhibits the peak rate constant, which is expected to be a weak function of λ ($k_{\text{et}}(E_0) \propto \lambda^{-1/2}$). The reorganization energy, λ , is found to be more or less 0.7 eV for all the AP derivatives because the molecular radius of the AP derivatives is almost the same size (ca. 0.35 nm, see Fig. S5 in the ESI†).²⁵

The dependence of k_{\max} on E_{red} , depicted in Fig. 5, should be closely related to eqn (2) and (3). Therefore, it is important for us to consider the relative energy position between the CB edge and E_{red} (Fig. 6). There is a discrepancy between the CB edge of TiO_2 in ethanol (−1.15 V vs. SHE)²⁶ and E_{red} of the AP derivatives. The reduction potential of AP in an ethanol– H_2O (1:1) mixture was reported to be −1.42 V,²⁷ the value of which is considerably shifted toward the positive direction (+0.47 V) compared to that in acetonitrile (−1.89 V) listed in Table 1 and 2. Thus, E_{red} for other AP derivatives would also shift in the same direction in ethanol. However, even though the positive shift is taken into consideration, the E_{red} of AP in ethanol (−1.42 V) is located at a more negative potential than the flatband potential in the dark (−1.15 V vs. SHE),²⁶ which is almost comparable with the CB edge of TiO_2 . Even

if the CB edge of TiO_2 under UV irradiation slightly shifts towards the negative direction because of the electron accumulation in the CB and at the Ti_{st} sites, the E_{red} of AP (-1.42 V) is still negatively positioned compared to the CB edge of TiO_2 . This implies that some AP derivatives with negative E_{red} values (e.g. 4–7) cannot be reduced on UV irradiated TiO_2 , which is, of course, not true. An interesting question is how the AP derivatives, especially substrates 4–7 possessing negative E_{red} values, can be hydrogenated on the TiO_2 surface. The adsorption model of the η_1 geometry may offer a reasonable explanation for the further positive shift of E_{red} of the AP derivatives because the interaction between the carbonyl oxygen atom and the surface Ti^{4+} sites induces an electron deficiency in the π -electron system and lowers the π^* LUMO level of the AP derivatives. Consequently, the adsorbed AP derivatives can be reduced by the electrons trapped at the Ti_{st} sites on the TiO_2 surface. The effect of adsorption on the positive shift of E_{red} would be greater for AP 5 because of its strongest adsorption property (see Table 1). Thus, the effect of adsorption on the positive shift of E_{red} can lead to the enhancement of the electron transfer efficiency on the TiO_2 surface.

On the basis of the above consideration, the relative energy position between the CB edge and E_{red} can be reasonably illustrated in Fig. 6, where E_{red} varies depending on the AP derivatives whereas λ can be fixed to be *ca.* 0.7 eV.²⁵ Therefore, the Gaussian curves of the acceptor and donor levels shown in Fig. 6 move upward and downward with the change in E_{red} but without a significant change in the shape. This means that a large number of Ti_{st} sites are accessible to the electron transfer for the AP derivatives with a positive E_{red} (e.g. 1–3) while the number of available Ti_{st} sites is limited for those possessing a negative E_{red} (e.g. 6, 7). The proportion of accessible Ti_{st} sites should be related to the percentages listed in Table 2. Here, the fluctuating acceptor level

(the Gaussian curve) of TFAP 1 would entirely cover the whole range of the electronic energy of Ti_{st} states within the band gap, thereby attaining a percentage of 100%. Thus, this model can satisfactorily explain the k_{max} dependence on E_{red} as well as the relationship between k_{max} and the amount of reacted electrons shown in Fig. 5, though the numerical analysis of this model seems to be difficult since the individual contributions of $k_{\text{et}}(E)$ (eqn (3)) are convoluted in eqn (2). The Marcus inverted region²³ was not observed in our reaction system because of two reasons: 1) the considerably negative E_{red} of the AP derivatives, *i.e.*, an insufficient driving force for this reaction and 2) the widely distributed Ti_{st} states within the band gap (1 eV more or less).⁹

In the photocatalytic hydrogenation of AP, the maximum reaction rate, k_{max} , increased with increasing incident light intensity, I .⁴ Therefore, the photo-hydrogenation of AP proceeds in a light-limited controlled manner. Since the excited electrons in the CB rapidly migrate and distribute to the Ti_{st} sites (within 500 ps even for the deep trap sites),^{28,29} the concentration of excited electrons accessible to the reaction should be related to the light intensity. The intensity dependence on k_{max} can be formulated in $k_{\text{max}} \propto I^n$,^{30–32} where n is usually taken from 0.5 to 1.0 depending on the light intensity. At a high light intensity, n is 0.5 because the Ti_{st} sites are saturated by the excited electrons and the band to band e^- - h^+ recombination becomes dominant (second order). At a very low light intensity, n is 1.0 because the Ti_{st} sites are not saturated and therefore the e^- - h^+ recombination *via* the Ti_{st} sites becomes first order. The intensity dependence on k_{max} for AP was in proportion to $I^{0.68}$ ($n = 0.68$), indicating that both the band to band recombination and the recombination *via* the Ti_{st} sites occur simultaneously.

Finally, we propose a reasonable reaction mechanism, depicted in Fig. 7. First, the adsorbed AP species (most likely

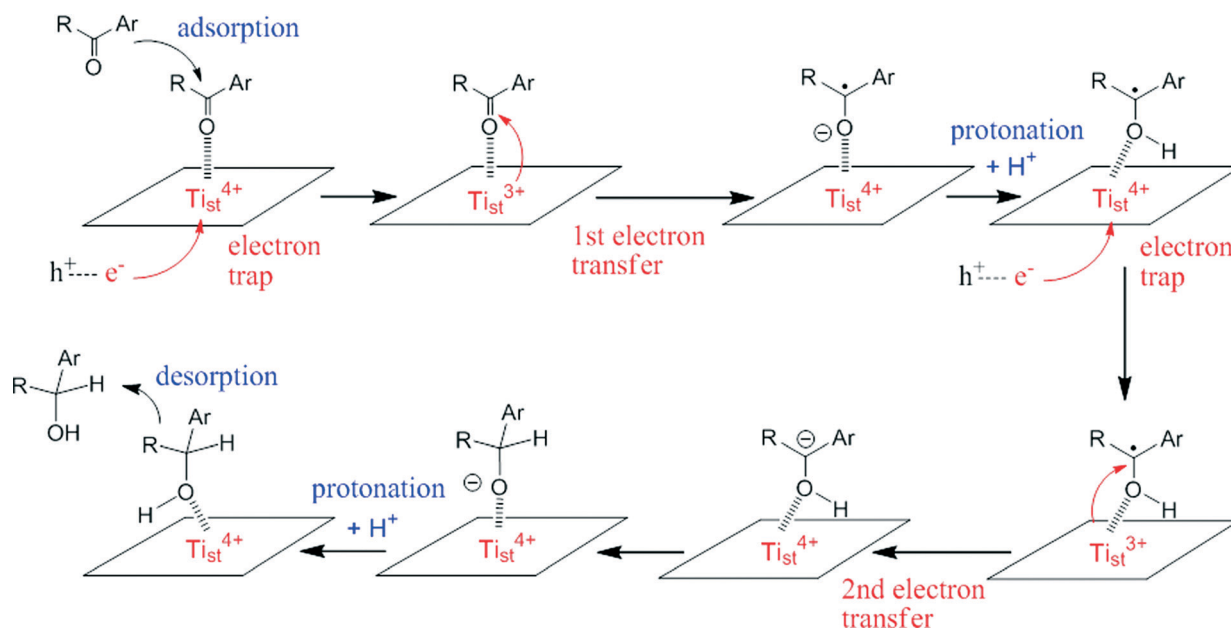


Fig. 7 A proposed reaction mechanism for the photo-hydrogenation of AP derivatives on the TiO_2 surface.

η_1 geometry) are reduced by the accumulated electrons to the anionic species through the first electron transfer step, which is strongly affected by the relative position of E_{red} . In this step, the trapped electrons seem to be transferred from the Ti 3d orbital to the π^* orbital on the carbonyl moiety. The next protonation step should be prior to the back electron transfer from the anionic species to the deep Ti_{st} sites because the trapped electrons at the deep Ti_{st} sites mostly remain, or even if the trapped electrons are consumed by the reaction, another electron can be rapidly supplied from the accumulated CB electrons within 500 ps (Fig. 6).^{28,29} This protonation step may be associated with the ethanol oxidation by h^+ on the TiO_2 surface. Recently, Morris *et al.* proposed the photo-oxidation mechanism of methanol on rutile TiO_2 nanoparticles by means of FT-IR spectroscopy, in which the photogenerated holes play a crucial role in the methanol oxidation and produce H^+ and a new surface hydroxyl group, HO_{br}^- , during the reaction.³³ In a similar manner, H^+ and/or HO_{br}^- might be generated during the photo-oxidation of ethanol on the P25 TiO_2 surface and associated with the protonation reaction. The second electron transfer should be faster than the first one because the predicted reduction potential of the acetophenone ketyl radical (-1.59 V vs. SHE in CH_3CN calculated by a quantum chemical calculation)³⁴ is $+0.3$ V more positive than that of AP 5 (-1.89 V). At the end of the sequential reaction, the final secondary alcohol product would be formed *via* the rearrangement and the second protonation.

Conclusions

We have demonstrated that the photocatalytic hydrogenation of AP derivatives proceeds *via* the surface defect Ti (Ti_{st}) sites on the TiO_2 surface, where they are not only adsorption sites but also electron trap sites. Under UV irradiation, the electron transfer event at the Ti_{st} sites initiates the hydrogenation of AP derivatives, in which the reaction rate is strongly affected by the reduction potential (E_{red}) of the substrates. A reasonable electron transfer reaction model *via* the Ti_{st} sites (Fig. 6) is proposed in this study. The results provide good insight into valuable information about the reaction mechanism of the photo-hydrogenation of AP derivatives as well as the physicochemical properties of the Ti_{st} sites on the TiO_2 surface.

Acknowledgements

This work was supported by Grant-in-Aid for Scientific Research (no. 22590026 and 24590067) from the Japan Society for the Promotion of Science.

Notes and references

- 1 S. Kohtani, E. Yoshioka and H. Miyabe, in *Hydrogenation*, ed. Karamé, InTech, Rijeka, 2012, ch.12, pp. 291–308, (This is an open access chapter, DOI: 10.5772/45732), and references therein.

- 2 S. Kohtani, E. Yoshioka, K. Saito, A. Kudo and H. Miyabe, *Catal. Commun.*, 2010, **11**, 1049–1053.
- 3 S. Kohtani, S. Nishioka, E. Yoshioka and H. Miyabe, *Catal. Commun.*, 2014, **43**, 61–65.
- 4 S. Kohtani, E. Yoshioka, K. Saito, A. Kudo and H. Miyabe, *J. Phys. Chem. C*, 2012, **116**, 17705–17713.
- 5 S. Földner, R. Mild, H. I. Siegmund, J. A. Schroeder, M. Gruber and B. König, *Green Chem.*, 2010, **12**, 400–406.
- 6 Y. Shiraishi, Y. Togawa, D. Tsukamoto, S. Tanaka and T. Hirai, *ACS Catal.*, 2012, **2**, 2475–2481.
- 7 U. Diebold, *Surf. Sci. Rep.*, 2003, **48**, 53–229, and references therein.
- 8 T. L. Thompson and J. T. Yates, *Chem. Rev.*, 2006, **106**, 4428–4453, and references therein.
- 9 M. A. Henderson, *Surf. Sci. Rep.*, 2011, **66**, 185–297, and references therein.
- 10 M. A. Henderson, *J. Phys. Chem. B*, 2004, **108**, 18932–18941.
- 11 M. A. Henderson, N. A. Deskins, R. T. Zehr and M. Dupuis, *J. Catal.*, 2011, **279**, 205–212.
- 12 R. Wang, K. Hashimoto, A. Fujishima, M. Chikuni, E. Kojima, A. Kitamura, M. Shimohigashi and T. Watanabe, *Nature*, 1997, **388**, 431–432.
- 13 J. Li, *Chromatographia*, 2004, **60**, 63–71.
- 14 T. Beager, M. Sterrer, O. Diwald, E. Knozinger, D. Panayotov, T. L. Thompson and J. T. Yates, *J. Phys. Chem. B*, 2005, **109**, 6061–6068.
- 15 S. H. Szczepankiewicz, A. J. Colussi and M. R. Hoffmann, *J. Phys. Chem. B*, 2000, **104**, 9842–9850.
- 16 S. H. Szczepankiewicz, J. A. Moss and M. R. Hoffmann, *J. Phys. Chem. B*, 2002, **106**, 2922–2927.
- 17 S. H. Szczepankiewicz, J. A. Moss and M. R. Hoffmann, *J. Phys. Chem. B*, 2002, **106**, 7654–7658.
- 18 M. Takeuchi, G. Martra, S. Coluccia and M. Anpo, *J. Phys. Chem. C*, 2007, **111**, 9811–9817.
- 19 M. Takeuchi, J. Deguchi, S. Sakai and M. Anpo, *Appl. Catal., B*, 2010, **96**, 218–223.
- 20 S. Ikeda, N. Sugiyama, S. Murakami, H. Kominami, Y. Kera, H. Noguchi, K. Uosaki, T. Torimoto and B. Ohtani, *Phys. Chem. Chem. Phys.*, 2003, **5**, 778–783.
- 21 Y. Q. Gao, Y. Georgievskii and R. A. Marcus, *J. Chem. Phys.*, 2000, **112**, 3358–3369.
- 22 N. S. Lewis, *J. Phys. Chem. B*, 1998, **102**, 4843–4855.
- 23 T. W. Hamann, F. Gstrein, B. S. Brunshwig and N. S. Lewis, *J. Am. Chem. Soc.*, 2005, **127**, 7815–7824.
- 24 J. W. Ondersma and T. W. Hamann, *J. Am. Chem. Soc.*, 2011, **133**, 8264–8271.
- 25 The outer-sphere reorganization energy for the AP derivatives at the TiO_2 /ethanol interface can be estimated by the following equation:^{22–24}

$$\lambda = \frac{(\Delta zq)^2}{8\pi\epsilon_0} \left[\frac{1}{a} \left(\frac{1}{n_s^2} - \frac{1}{\epsilon_s} \right) - \frac{1}{2R} \left\{ \frac{1}{n_s^2} \left(\frac{n_{\text{TiO}_2}^2 - n_s^2}{n_{\text{TiO}_2}^2 + n_s^2} \right) - \frac{1}{\epsilon_s} \left(\frac{\epsilon_{\text{TiO}_2} - \epsilon_s}{\epsilon_{\text{TiO}_2} + \epsilon_s} \right) \right\} \right]$$

where Δz is the change in the charge of the AP derivative, a is the radius of the AP derivative (*ca.* 0.35 nm estimated using the DFT calculation), n_s and n_{TiO_2} are the refractive

- index of ethanol (1.36)²⁷ and anatase TiO₂ (2.5),²⁴ respectively, ϵ_s and ϵ_{TiO_2} are the static dielectric constant of ethanol (24.6)²⁷ and anatase TiO₂ (114),²⁴ respectively, and R is the distance from the adsorbed AP derivatives to the TiO₂ surface. Thus, we obtained the outer-sphere reorganization energy as 0.7 eV by assuming $R = a = 0.35$ nm. Although λ is the sum of the inner-sphere and outer-sphere components, λ should be more or less 0.7 eV because the calculated inner-sphere reorganization energy for organic dyes adsorbed on TiO₂ nanoparticles is reported to be negligibly small.³⁵
- 26 G. Redmond and D. Fitzmaurice, *J. Phys. Chem.*, 1993, **97**, 1426–1430.
- 27 M. Montalti, A. Credi, L. Prodi and M. T. Gandolfi, in *Handbook of Photochemistry*, CRC, Boca Raton, 3rd edn, 2006, ch. 7, pp. 493–527.
- 28 Y. Tamaki, A. Furube, M. Murai, K. Hara, R. Katoh and M. Tachiya, *Phys. Chem. Chem. Phys.*, 2007, **9**, 1453–1460.
- 29 Y. Tamaki, K. Hara, R. Katoh, M. Tachiya and A. Furube, *J. Phys. Chem. C*, 2009, **113**, 11741–11746.
- 30 U. Stafford, K. A. Gray and P. V. Kamat, *J. Catal.*, 1997, **167**, 25–32.
- 31 A. Mills, J. Wang and D. F. Ollis, *J. Phys. Chem. B*, 2006, **110**, 14386–14390.
- 32 A. Mills, J. Wang and D. F. Ollis, *J. Catal.*, 2006, **243**, 1–6.
- 33 D. A. Panayotov, S. P. Burrows and J. R. Morris, *J. Phys. Chem. C*, 2012, **116**, 6623–6635.
- 34 Y. Fu, L. Liu, H.-Z. Yu, Y.-M. Wang and Q.-X. Guo, *J. Am. Chem. Soc.*, 2005, **127**, 7227–7234.
- 35 E. Maggio, N. Martsinovich and A. Troisi, *J. Phys. Chem. C*, 2012, **116**, 7638–7649.